Enhanced electrochemiluminescent aptasensor for mercury based on CdTeSe@CdS QDs-DNA bioconjugates and enzymatic catalysis

*Jian-Jun Shi[1, *], Qian-Qian Zhang[1], Wei Hu[1], Ping Yang [1]*

School of Chemical Engineering, Anhui University of Science and Technology, Huainan, 232001, People's Republic of China
[*]E-mail: jjshi@aust.edu.cn

Heavy metals in atmospheric particulate matter emission from coal-fired power plants have attracted global attention. Aiming at the complexity and trace content of mercury, a highly sensitive and selective "signal-on" electrochemiluminescent (ECL) aptasensor was proposed for detection of mercury by using CdTeSe@CdS QDs-DNA bioconjugates and enzyme-catalysis signal amplification strategy. The thiol-modified DNA I (Probe I) was fixed on the gold electrode as the main chain, which reacted with QDs-labeled adapter probe DNA II (Probe II) by thymine-Hg^{2+}-thymine (T-Hg^{2+}-T) structure in presence of Hg^{2+}, resulting in the production of the increased ECL signal of QDs. The biotin-labeled DNA III (Probe III) was paired with Probe I, and streptavidin-horseradish peroxidase (HRP) conjugate integrated to Probe III to enhance the intensity of ECL by enzymatic catalysis. The ECL signal of CdTeSe@CdS QDs-DNA provides quantitative measures of the concentrations of Hg^{2+}, with a linear calibration ranging from 1.0×10^{-11} to 1.0×10^{-6} M. This ECL aptasensor performed with admirable stability and good selectivity, enabling the detection of mercury at a very low limit (3.5×10^{-12} M) and negligible for other interfering metal ions. The results suggested that this method is feasible and widely used to determine mercury in atmospheric particulate matter (such as fly ash), as well as the other heavy metals in the environment.

1. INTRODUCTION

Mercury, one of highly toxic and hazardous heavy metal pollution [1, 2], lies in water, soil, especially in the atmospheric particulate matter [3, 4]. Herein, Mercury in fly ash from coal-fired power plants mainly exists in the forms of gaseous elemental mercury (Hg^0), oxidized mercury (Hg^{2+}) and particle-bound mercury (Hg^p) [5], and there are four mercury speciation (HgS, HgO, $HgCl_2$, and

HgSO$_4$) [6]. Hg^{2+} is the main valence state, which tends to enter human's body via various paths and affect the neuroimmune systems, influence genes expression, resulting in serious harm to the health, even die at light concentrations [7-9]. Emissions of hazardous trace elements in China are of great concern because of their negative impacts on local air quality as well as on regional environmental problem and ecological balance. The World Health Organization (WHO) and the US Environmental Protection Agency (EPA) have adopted an acceptable lowest concentration of Hg^{2+} at 10 nM in the table-water [10,11]. The Minamata Convention on Mercury was beginning to take effect since 2017 to accelerate actions on controlling mercury emissions [12].

Thus, various analytical protocols and methods were used to detect trace mercury in the environment, including fluorescence sensor [13,14], light-addressable potentiometric sensor [15], and electrochemical sensor [16,17]. Herein, electrochemical biosensors, a subset of chemical sensors, have received considerable attentions due to their low cost, fast detection time and high sensitivity, highly specific biological identification processes. These devices include biometric elements, such as enzymes, proteins, antibodies, and so on, which could react with the target analytes selectively and generate an electrical signal that is related to the analyte concentration in the study [18]. It is worth noting that functional aptamer sensors have received considerable interest in mercury detection because of the synthetic repeatability, reversible degeneration and easy to transduce signals [19]. Mercury ions are easily to bind specificity with thymine-rich (T-rich) DNA sequences (called Hg^{2+} aptamers) to form stable T-Hg^{2+}-T complex, which can be used to construct sensors for highly selective Hg^{2+} determine. The current researched the T-rich nucleic acid sensors for Hg^{2+} detection based on core-shell Ag@SiO$_2$ nanoparticles [20], structure-switching DNA [21], gold nanoclusters [22, 23] and quantum dots (QDs) [24]. For example, Itamar Willner et. al [25] have reported on the use of T-rich nucleic acid functionalized QDs for the selective analysis of mercury ions by using an electron-transfer-quenching path.

Electrochemiluminescence (ECL), also called electrogenerated chemiluminescence, which certain voltage or current signal on the electrode surface exergonic high-energy electron transfer reaction to form excited states that produce chemical luminescence. There are three types of luminophores in ECL system including ruthenium (II) complexes, luminol, and QDs. ECL system based on QDs or semiconductor nanocrystals (NCs) has generated an intense area of research interest in recent years [26,27], in which near-infrared QDs (NIR-QDs), such as CdSeTe [28], InAs [29], PbSe [30] and CuInS [31], especially stood out. The alloy CdSeTe QDs have attracted widespread attention since 2003 [32]. Nowadays, there are varieties of methods have been developed for the preparation of CdTeSe QDs [33-36]. However, CdTeSe QDs surface has a large number of defects and unsaturated suspension keys that cause a low fluorescence efficiency. Therefore, it is of great significance to develop new processing method that CdTeSe QDs covers with a wide band gap of an inorganic material to reduce surface defects for preparation NIR-emitting core-shell CdTeSe QDs with excellent optical properties.

Herein, we developed ECL aptasensor for sensitive and selective detection of the trace content of mercury in complex environmental samples by using core-shell CdTeSe@CdS QDs-DNA bioconjugates and enzyme-catalysis signal amplification strategy.

2. EXPERIMENTAL

2.1 Materials

All biochemical agents were purchased from the Sigma-Aldrich Company (the United States), including streptavidin horseradish peroxidase conjugate (HRP), N-hydroxy-succinimide (NHS), 1-ethy-3-(3-dimethylaminopropyl) carbodiimide hydrochloride (EDC), 6-mercapto-1-hexanol (MCH). selenium powder (Se) and tellurium powder (Te) and 3-mercaptopropionic acid (MPA) were obtained from Acros Organics (New Jersey, USA). Cadmium chloride ($CdCl_2 \cdot 2.5H_2O$) and sodium borohydride ($NaBH_4$) were purchased from Tianjin Chemical Research Institute (Tianjin, China). Disodium hydrogen phosphate (Na_2HPO_4), sodium dihydrogen phosphate (NaH_2PO_4), sodium hydroxide (NaOH) and hydrochloric acid (HCl) were obtained from Nanjing Chemical Reagents Factory (Nanjing, China). The PBS (pH 7.4) solution contained 0.1 M Na_2HPO_4 and 0.1 M NaH_2PO_4. The electrolyte was 5 mL PBS solution with 0.1 M $K_2S_2O_8$ and 0.1 M KCl for ECL measurements. The solution containing 0.1 M KCl and 50 mM $K_3[Fe(CN)_6]/K_4[Fe(CN)_6]$ ($[Fe(CN)_6]^{3-/4-}$) was applied to electrochemical impedance spectroscopy (EIS) characterization. All other reagents were of analytical reagent grade and used without further purification. Millipore ultrapure water (resistivity $\geq$ 18.2 MΩ cm) was employed throughout the experiment.

Three oligonucleotides sequences used are given below: the thiol-modified capture probe DNA I (Probe I, PI): 5'-HS-$(CH_2)_6$-AAAAAGGTTGTTGGGGAGTGAGTGAGT-3', the amine-modified target probe DNA II (Probe II, PII): 5'-NH_2-$(CH_2)_6$-AAAAAAAAAAAAAAACCCTTCTT-CC-3', biotin-modified the complementary probe DNA III (Probe III, PIII): 5'-biotin-AAAAAAA-AAAACTCACTCACTC-3'. All labeled DNA chain were purchased from Shanghai Sangon Biotechnology Co. Ltd. (Shanghai, China).

2.2 Synthesis of CdTeSe@CdS QDs

The synthesis of CdTeSe QDs referred to the method reported previously [37]. Briefly, 50 mL $CdCl_2$ solution (5 mmol) and 37 µL MPA was mixed under nitrogen protection, and adjusted pH to 12.0-12.5 by adding 1 M NaOH solution. Then the freshly prepared NaHTe and NaHSe mixture solution (Te/Se = 1:4) was injected into the above $CdCl_2$-MPA solution. The amount of Cd was over 20-fold of Te and Se. The mixture solution was refluxed under nitrogen atmosphere at room temperature for about 1h to obtain CdTeSe QDs.

The CdTeSe@CdS QDs can be facilely obtained by further treatment of CdTeSe QDs solution with $CdCl_2$ (5 mM) and MPA (40 µL) was adjusted pH to 12.0-12.5 by the addition of 1 M NaOH solution, then react under microwave radiation power of 640 W for a certain time. The obtained MPA modified CdTeSe@CdS QDs (MPA-CdTeSe@CdS) solution was purified to remove the superfluous MPA and stored in the dark at 4 °C for later use. The carboxyl MPA-capped QDs (10 µL, 2.4 µM) was activated by 10 µL (4.2 mg mL^{-1}) of EDC and 5 µL (2.1 mg mL^{-1}) of NHS for 15 min. The obtained carboxyl group modified CdTeSe@CdS QDs (COOH-QDs) possessed an ultra-strong fluorescence and a good stability in PBS solution.

2.3 Preparation of the ECL aptasensor
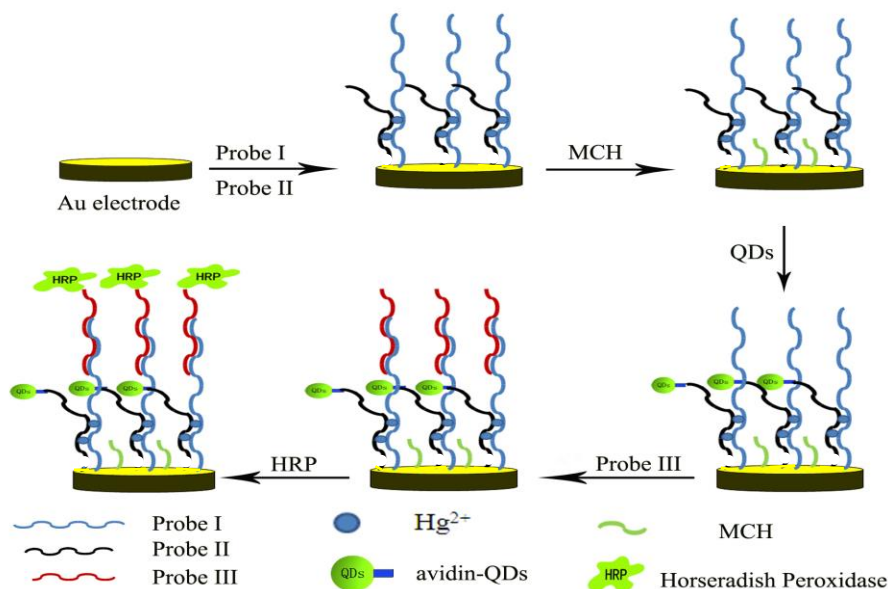
Scheme 1. The fabrication of ECL aptasensor

The process of ECL aptamer sensor assemble are shown in Scheme 1. The gold electrode was rinsed prior in Piranha solution (30% H_2O_2: 98% H_2SO_4 =3:7, V/V) for 5 min twice and then cleaned with water before use. All the oligonucleotides solutions were heated to 90 °C for 3 min and then cooled in ice for 10 min before use. For the synthesis of ECL aptasensor, thiolated-PI solution (20 µL, 1 µM) was unfolded at the disposed Au electrode for incubate 12 h at 37 °C in the 100% humidity and self-assembled through Au-SH bond. Then the electrode was immersed with MCH (1 mM, 100 µL) for 2 h to remove the non-specific adsorption of PI and MCH can also fill the surface of the electrode. Next, it was covered with the as-prepared COOH-QDs conjugate with NH_2-modified PII (20 µL) to form QDs-aptamer PII and through T-Hg^{2+}-T structure combine to PI for incubated 2 h by using the ECL property of QDs to produce the ECL signal. Then the target PIII solution of biotin-marked (20 µL) was added to the modified electrode to match the base complement with PI chain for 2 h. The avidin-labeled HRP enzyme solution (20 µL) was dropped on the electrode for reaction 1 h, which combined with the complementary PIII by biotin-avidin reaction to enhance the intensity of the ECL by the enzymatic catalysis. After each step of self-assembled, the electrode was completely washed with deionized water. The obtained HRP/PIII-QDs/PII/Hg^{2+}/PI/Au electrode was used for the subsequent experiments.

2.4 Apparatus and Characterization

Transmission electron microscopy (TEM) and high-resolution transmission electron microscopy (HRTEM) images were observed by JEOL-2100 microscope for the sample morphology analysis. UV-Vis spectra were recorded on UV-3600 spectrophotometer (Shimadzu, Kyoto, Japan) and

photoluminescence (PL) spectra were obtained on RF-540 spectrophotometer (Shimadzu, Kyoto, Japan). The EIS and CV analyses were performed on Autolab PGSTAT12 (Ecochemie, BV, Netherlands). The EIS characterization was carried in 10 mM PBS (pH 7.4) containing 10 mM $K_3[Fe(CN)_6]/K_4[Fe(CN)_6]$ and 0.1 M KCl with the frequency range of $10^{-1} \sim 10^5$ Hz. In all electrochemical experiments, the conventional three-electrode system was employed with a modified Au electrode as the working electrode, a saturated calomel electrode (SCE) as the reference electrode, and a platinum wire as the counter electrode.

2.5 ECL measurements

The ECL measurements were performed in a 5-mL glass cell. The electrolyte was 0.1 M pH 7.4 PBS containing 0.1 M KCl and 0.1 M $K_2S_2O_8$. The potential range applied to the Au disk working electrode (2 mm diameter) in the CV measurement was from 0 to -1.5 V at 100 mV s^{-1}. The ECL emission intensity (I_{ECL}) corresponding to CV measurements was recorded by the MPI-E multifunctional electrochemiluminescence analyzer (Xi'an Remex Analysis Instrument Co., Ltd., Xi'an, China) at room temperature. The emission window was placed in front of the photomultiplier tube (PMT), which was set at 600 V.

3. RESULTS AND DISCUSSION

3.1 Characterization of CdTeSe@CdS QDs

Typical TEM, HRTEM images, SAED pattern and EDS for the MPA-coated CdSeTe@CdS QDs are shown in Fig.1. The TEM image of CdSeTe@CdS QDs (Fig. 1A) shows that the QDs have a uniform size and regular shape. From the HRTEM image (Fig. 1B), we found that the CdSeTe@CdS QDs have a good crystal structure and are monodispersed. The CdSeTe@CdS QDs with a zinc-blende crystal structure were prepared in aqueous solution and the lattice spacing of 0.348 nm corresponded to the (111) plane of CdSeTe@CdS QDs, which was marked in Fig. 1B. The corresponding SAED pattern (Fig. 1C) exhibits rings, which could be assigned to the diffraction from (111), (221), and (311) planes of zinc-blende crystal structure. The particle size distribution was further evaluated by using Mastersizer Laser Particle Size Analyzer. The average size of the nanocrystals was around 5 nm, which is consist with the result observed from the TEM image, which slight larger than the previous report CdSeTe QDs [32], due to the crystal growing of the CdS shell [38]. The EDS spectra of CdSeTe@CdS QDs (Fig. 1D) confirmed the presence of cadmium, selenium, tellurium and sulfur. Moreover, Cd:Se:Te:S is equal to 100:1.9:11.4:160 for CdSeTe@CdS QDs. **1**
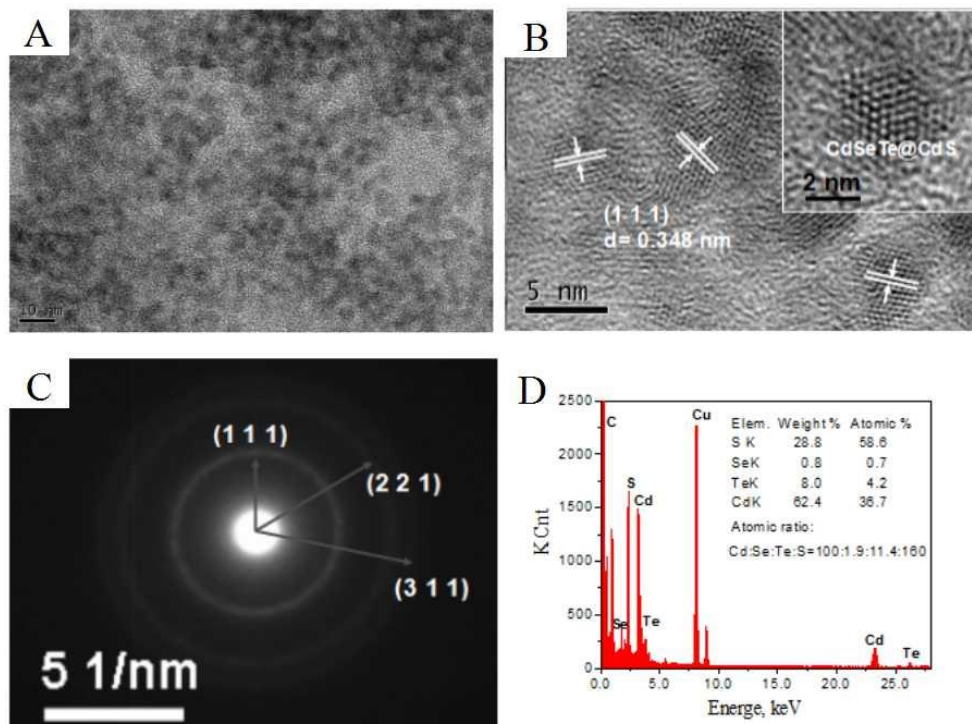
Figure 1. TEM image of CdSeTe@CdS QDs (A); HRTEM image of CdSeTe@CdS QDs (B); SAED
pattern of the elements of CdSeTe@CdS QDs (C); and EDS image of CdSeTe@CdS QDs (D).
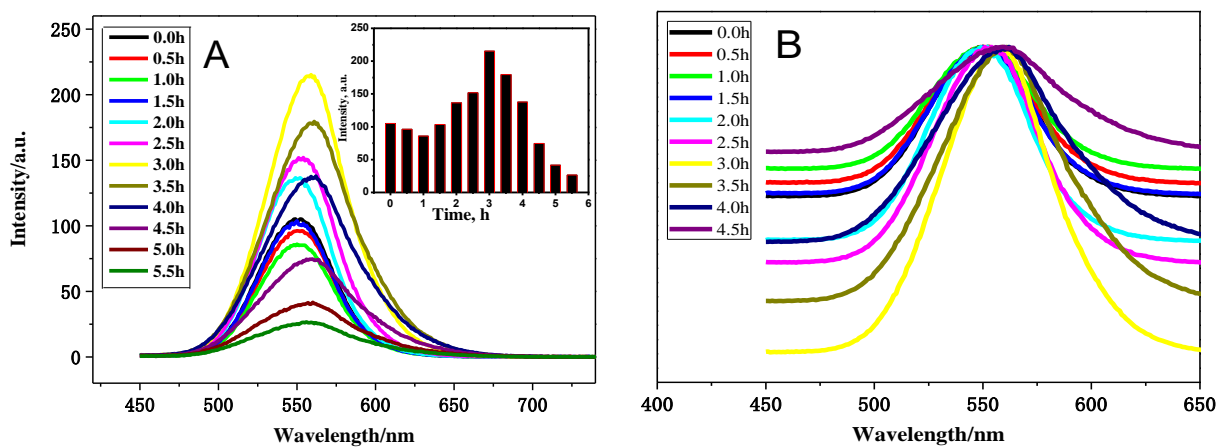

Figure 2. Fluorescence spectra of the CdTeSe@CdS QDs with the excitation wavelength of 440 nm
(A) in different microwave reaction times from 0 h to 5.5 h and (B) Fluorescence spectra
normalized curve of the CdTeSe@CdS QDs in different microwave reaction times from 0 h to
4.5 h.

The fluorescence spectra of CdTeSe@CdS QDs obtained after different microwave reaction
times were shown in Fig. 2. The core-shell structured CdTeSe@CdS QDs exhibited the fluorescence
peak centered at 557 nm (excitation wavelength 439 nm) as shown in Fig. 2A. The microwave reaction
for 3 h obtained a maximum fluorescence intensity due to the thickness of the CdS shell increased to a
critical threshold [39]. Therefore, the following microwave reactions were carried out at 3 h. As
depicted fluorescence spectra normalized curve in Fig. 2B, the fluorescence emission wavelength has a

550-nm red shift with the increase of reaction time. This result can be attribute to the growth of the CdS shell to form new defects that cause the changes in PL intensity [39].

3.2 Electrochemical impedance spectroscopy of the aptasensor

Electrochemical impedance spectroscopy (EIS) is a powerful technique for investigating the features of surface-modified electrodes. The change of electron transfer resistance (R_{et}) could reflect the different modification processes that occur on the electrode surface. Fig.3 shows the change of the EIS for the entire surface modification of the electrode. Compared with bare Au electrode (curve a), the association of PI on the electrode resulted in high impedance of 600 cm^2 (curve b), mainly due to the electrostatic repulsion between negative charges of the DNA aptamer and the $[Fe(CN)_6]^{3-/4-}$ ions, which hindering the electrochemical redox probe $[Fe(CN)_6]^{3-/4-}$ rate of electron transfer on the electrode and leading to enhance the electrode impedance values [40]. The PII was linked with the PI (curve c) by base-pairing hybridization, which generated a weak electron transfer and bring about supreme semicircle domain. Introducing semiconductor nanomaterials on the modified electrode (curve d) caused system's electroconductivity enhancement and the electrode R_{et} sharply decreases, but after the addition of PIII (curve e) on electrode lead to impedance increases again. When the probe chain modified on electrode was immersed in the HRP enzyme solution (curve f), the R_{et} was greatly reduced, indicating the formation of the aptamer-HRP complex. Through the representation of the EIS, the process and efficiency of the layers of the electrode surface are clearly visible, which are quite in accord with effects of biomolecular and semiconductor QDs on the EIS result in our previous report [41].
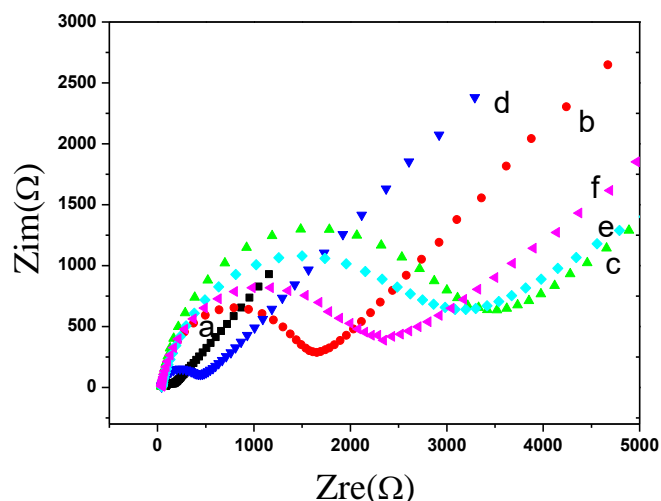
Figure 3. Nyquist plots corresponding to the different stages of electrode modification in 0.1 M KCl + 2 mM $[Fe(CN)_6]^{3-/4-}$. The EIS frequency range: $0.1–1.0\times10^5$ Hz. (a) bare Au electrode, (b) PI/Au electrode, (c)PII/Hg^{2+}/PI/Au electrode, (d) QDs/PII/Hg^{2+}/PI/Au electrode, (e) PIII-QDs/PII/Hg^{2+}/PI/Au electrode, (f) HRP/PIII-QDs/PII/Hg^{2+}/PI/Au electrode.
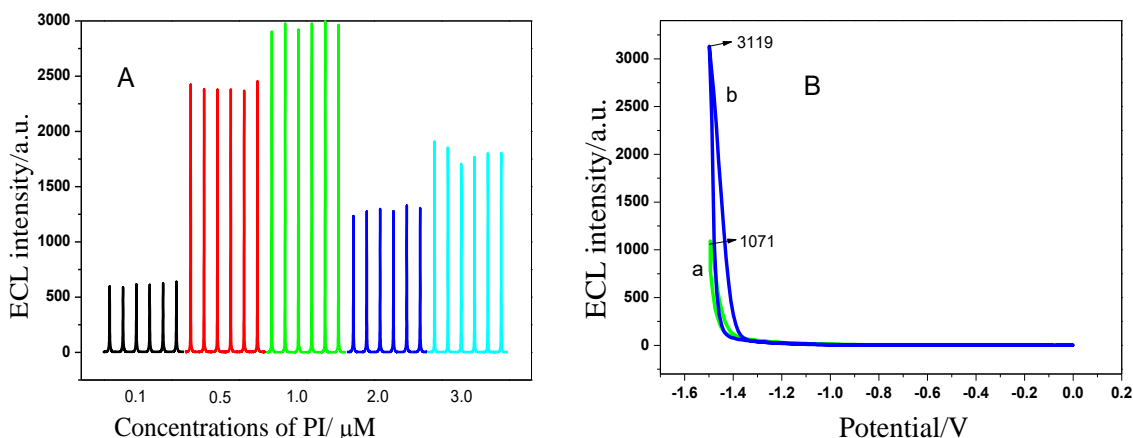
Figure 4. (A) The ECL intensity in presence of different concentrations of PI; (B) ECL-potential curve of PIII-QDs/PII/Hg^{2+}/PI/Au electrode before (a) and after (b) assembled the HRP

3.3 Electrochemiluminescence of the aptasensor and calibration curve

In the assembled process of sensor, the main chain PI determines the signal response of the entire sensor on the electrode surface. To explore optimal ECL intensity, experiment conditions of different PI concentrations were examined, as shown in Fig. 4A, the ECL intensity was affected dramatically. With the increasing of PI concentration from 0.1 μM to 1.0 μM and resulting in the increase of ECL intensity to a maximum value, which attributed to the saturated concentration of the base pairing between PII, PIII and PI. Then the ECL intensity reduced obviously when PI concentration was more than 1.0 μM due to the Steric Hindrance Effect on the following hybridization steps [42]. In the experiment, the concentration of 1.0 μM PI was chosen as the optimal concentration.

Fig. 4B shows the impact of HRP enzyme on sensors. The avidin-labeled HRP and PIII chains of biotin are linked by the specificity of biological and affinity. In 5 mL 100 mM PBS containing 0.1 M $K_2S_2O_8$ and 0.1 M KCl or 5 mL 1.0×10^{-6} M H_2O_2 detection system for ECL test, the result demonstrated the ECL response increased significantly by about 65.7% (from 1071 to 3119 a.u.) in presence of HRP, which illustrated enzymatic catalysis makes an increase number of free radicals in the system and these free radicals are more easily touch to the excited state of QDs, resulting in the increasing the ECL intensity. The enhancement effects of enzyme-catalysis on the signal amplification have also been confirmed in an ECL immunosensor by Wei [43].

Under the optimum conditions, the ECL intensity of the experiment was detected after adding varying concentrations of Hg^{2+}. Fig. 5 shows that the ECL intensity was enhanced along with the increase of the Hg^{2+} concentration. A linear relationship between the ECL intensity and the logarithm of the concentration of Hg^{2+} was achieved in the range from 1.0×10^{-11} M to 1.0×10^{-6} M with the equation $I_{ECL} = 7976.33 + 726.12 \log c_{Hg^{2+}}$ ($R^2 = 0.9912$), where the R^2 is regression coefficient and the detection limit is 3.5×10^{-12} M (S/N=3), which is well below the minimum level of mercury at 10 nM permitted by the WHO and the EPA. The proposed sensor exhibited a wider detection range and lower detection limit than the previous methods as shown in Table 1. As the target Hg^{2+} concentration

enlarge, the corresponding sensor's ECL strength response enhance, which manifested the T-Hg^{2+}-T structure was formed largely by combining QDs-PII chain with PI on Au electrode.
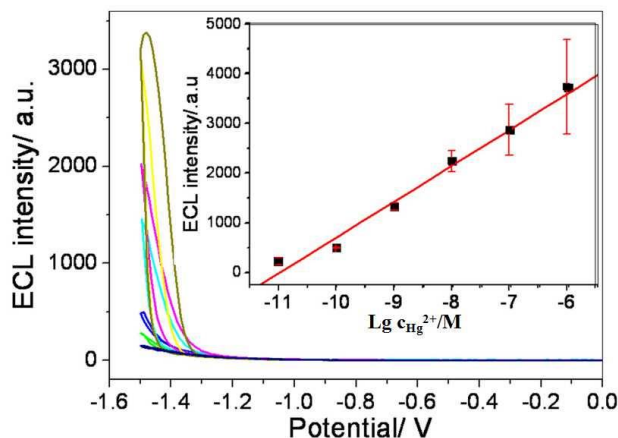
Figure 5. ECL intensity for the detection of different concentrations of Hg^{2+}. From bottom to top (a-g): 0 M, 10^{-6} M, 10^{-7} M, 10^{-8} M, 10^{-9} M, 10^{-10} M, 10^{-11} M. Inset: Linear relationship between the ECL intensity and the logarithm of the concentration of Hg^{2+}. The measurements were conducted in PBS buffer solution (pH 7.4) containing 0.1 M KCl and 0.1 M K$_2$S$_2$O$_8$ with the scan rate of 100 mV s^{-1} and the voltage of the photomultiplier tube was 600 V.
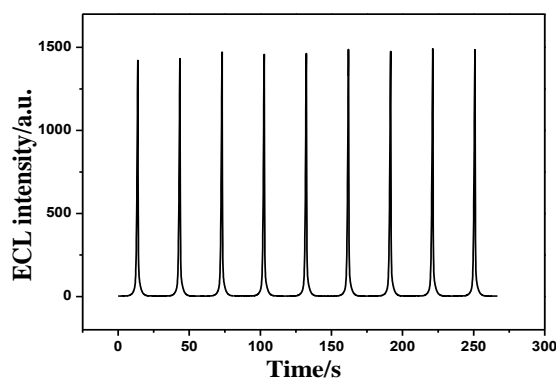
Figure 6. ECL-potential curve of HRP/PIII-QDs/PII/Hg^{2+}/PI/Au electrode under continuous cyclic voltammetry scans

Table 1. Comparison of the proposed method with some of the previously reported methods in the determination of mercury. LOD: limit of detection

Methods	Linear range(M)	LOD(M)	Reference
FL (aptamer-Ag@SiO$_2$ NPs)	1.2×10^{-9} - 1.4×10^{-8}	3.3×10^{-9}	[20]
FL (structure-switching DNA)	3.0×10^{-9} - 8.0×10^{-7}	3.2×10^{-9}	[21]
FL (DNA-templated Au NCs)	1.0×10^{-13} - 1.0×10^{-11}	5.0×10^{-8}	[23]
ECL (HRP/PIII-QDs/PII/Hg^{2+}/PI)	1.0×10^{-11} - 1.0×10^{-6}	3.5×10^{-12}	This work

3.4 Stability of the ECL aptasensor

Furthermore, the stability of the aptasensor was investigated. The ECL measurement of the modified electrodes was performed in 5 mL 100 mM PBS (pH 7.4) containing 0.1 M $K_2S_2O_8$ and 0.1 M KCl electrolyte in the presence of 10^{-9} M Hg^{2+}. As shown in Fig. 6, ECL signals remain stable and high intensity under continuous cyclic voltammetry scans of 300 s. It can be attributed to the effective step-by-step assembly of the sensor interface. Namely, PI chains are securely assembled to the Au electrode surface through the Au-S bond [17]. PII chains are labeled with QDs by EDC/NHS amidation reaction, and successful hybridized with PI chains via the formation of T-Hg^{2+}-T structure in the presence of mercury ions. The PIII chains are base-pairing hybridized with PI chains and formed stable Watson-Crick double helix. The avidin labeled HRP-enzymes are bonded to 5'-biotin modified PIII chains by biotin-avidin reaction as well.

3.5 Selectivity of the ECL aptasensor

The selectivity and specificity of the proposed ECL aptasensor was studied via contrast experiments in the presence of probably co-exist metal ions of fly ash sample, such as Mg^{2+}, Cd^{2+}, Fe^{2+}, Al^{3+}, Pb^{2+}, Ag^+ and Mn^{2+}. Fig. 7 shows the ECL intensity response to Hg^{2+} is much higher than other metal ions under the same experimental conditions. It shows that the base T are easier and more specific to combine Hg^{2+} than other metal ions to form T-Hg^{2+}-T configuration between the PII chain and PI chain [20-22]. The experimental results show that the ECL biosensor has a specific recognition function to Hg^{2+}.
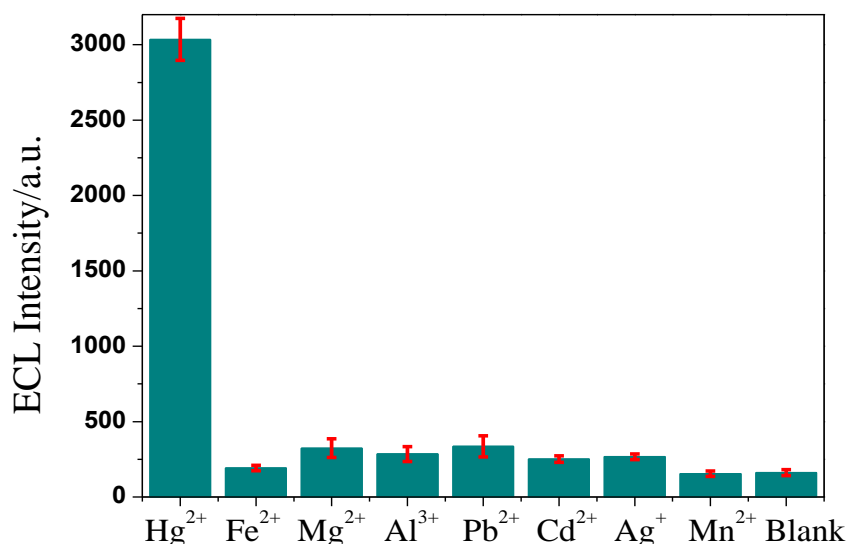
Figure 7. Selectivity in the analysis of mercury by the ECL aptasensor. The concentration of each metal ion was 1 μM in 0.1 M PBS containing 0.1 M $K_2S_2O_8$. ECL signal changes of various metal ions (all at 10^{-6} M) (Mg^{2+}, Cd^{2+}, Fe^{2+}, Al^{3+}, Pb^{2+}, Ag^+, Mn^{2+}, Hg^{2+}). Experimental conditions as in Figure 1. The incubation time for all ions was 1 h.

3.6 Application of the ECL aptasensor for mercury in fly ash

First, the samples of the fly ash (Coal Power Plant of Huainan) were sieved to 200 meshes for acidizing-digestion by modified previous method [44] as follows: 0.1 g of fly ash samples were added to Teflon lined stainless-steel autoclave, then added 5 mL of nitric acid, 2.5 mL of hydrochloric acid, 0.3 mL hydrogen peroxide and 1.0 mL of hydrofluoric acid successively. The autoclave was heated at 120 °C and maintained for 1 h, and allowed to cool to room temperature. The mercury in various forms could be completely converted to Hg^{2+} by the H_2O_2-HF enhanced digestion in a far shorter time than the conventional HNO_3-HCl digestion method [45]. After being diluted to 100-mL by deionized water, the mercury content was determined by atomic fluorescence spectra according to the previous determine method [46]. The results of the determination of mercury in actual fly ash samples were shown in Table 2.

The pH of digestion solutions of the fly ash was adjusted to neutral, diluted the fly ash solution to the linear range of $10^{-11} \sim 10^{-6}$ M and fixed experimental concentrations of Hg^{2+} at 1.50×10^{-10} M to build ECL biosensor detection. As seen in Table 3, the consequence revealed an admissible RSD less than 5%, which indicated that the proposed sensor is available to apply for recognizing Hg^{2+} in real fly ash samples. The mercury in the fly ash was determined by standard curve method. The linear regression equation was $I_{ECL} = 7976.33 + 726.12 \lg c_{Hg}^{2+}$ to calculate the concentration of mercury.

Table 2. Determination of Hg^{2+} in the fly ash by atomic fluorescence spectroscopy

Number	Hg^{2+} content（ng ml^{-1}）	Hg^{2+} concentration（M）
1	0.602	3.00×10^{-9}
2	0.624	3.12×10^{-9}
3	0.455	2.20×10^{-9}

Table 3. The ECL detection of Hg^{2+} in fly ash by standard curve method.

Number	Concentrations of mercury (M)	ECL Measured value	Concentrations of mercury Calculated value	relative standard deviation (RSD)%
1	1.5×10^{-10}	790	1.30×10^{-10}	
2	1.5×10^{-10}	815	1.37×10^{-10}	2.6
3	1.5×10^{-10}	810	1.34×10^{-10}	

4. CONCLUSION

In summary, a highly sensitive and selective electrochemiluminescent aptasensor for mercury ions has been constructed based on the QDs-aptamer bioconjugate and enhanced effects of enzymatic catalysis. Herein, CdTeSe@CdS QDs-DNA bioconjugates was designed as recognition probe, thiol-modification of adapter Probe I as the main chain. In presence of Hg^{2+}, stable T-Hg^{2+}-T complex was

generated, and the ECL of QDs can be detected. The quantification of Hg^{2+} was accomplished in the range from 1.0×10^{-11} M to 1.0×10^{-6} M with a detection limit of 3.5×10^{-12} M (S/N=3). Meanwhile, the biosensor can distinguish Hg^{2+} from other metal ions with high selectivity. Furthermore, the proposed sensing strategy can be feasible and widely used to detect other heavy metals in the complex environmental samples.

References

1. Q.R. Wang, D. Kim, D.D. Dionysiou, G.A. Sorial, D. Timberlake, *Environ. Pollut.*, 131 (2004) 323.
2. A. Afkhami, F.S. Felehgaria, T. Madrakiana, H. Ghaedi, M. Rezaeivala, *Anal. Chim. Acta.*, 771 (2013) 21.
3. S. Pongpiachan, S.X. Liu, R.J. Huang, Z.Z. Zhao, J. Palakun, C. Kositanont, J.J. Cao, *Arch. Environ. Con. Tox.*, 72 (2017) 364.
4. P. Gao, T.T. Lei, L.M. Jia, Y. Song, N. Lin, Y.Q. Du, Y.J. Feng, Z.H. Zhang, F.Y. Cui, *Sci. Total Environ.*, 576 (2017) 628.
5. F.Y. Wang, S.X. Wang, Y. Meng, L. Zhang, Q.R. Wu, J.M. Hao, *Fuel,* 163 (2016) 232.
6. P. He, X.B. Zhang, X.L. Peng, J. Wu, X.M. Jiang, *Fuel Process. Technol.*, 142 (2016) 6.
7. D. Suvd, R. Davaadorj, D. Baatartsol, S. Unursaikhan, M. Tsengelmaa, T. Oyu, S. Yunden, A.M. H. Rogers, *Procedia. Environ. Sci.*, 30 (2015) 97.
8. M.N. Elizabeth, J.L. Stephen, *Chem. Rev.*, 108 (2008) 3443.
9. J.H. Huang, X.F. Su, Z.G. Li, *Biosens. Bioelectron.*, 96 (2017) 127.
10. P. Liang, D.D. Shao, S.C. Wu, J.B. Shi, X.L. Sun, F.Y. Wu, S.C.L. Lo, W.X. Wang, M.H. Wong, *Chemosphere.*, 82 (2011) 1038.
11. H. Wang, Y.H. Zhang, H.M. Ma, X. Ren, Y.G. Wang, Y. Zhang, Q. Wei, *Biosens. Bioelectron.*, 86 (2016) 907.
12. Minamata Convention on Mercury website, http://www.mercuryconvention.org/.
13. L. Deng, Z.X. Zhou, J. Li, T. Li, S.J. Dong, *Chem. Commun.*, 47 (2011) 11065.
14. L.B. Li, B. Yu, T.Y. You, *Biosens. Bioelectron.*, 74 (2015) 263.
15. C. Shao, S. Zhou, X.B. Yin, Y.J. Gu, Y.F. Jia, *Sensors.*, 16 (2016) 701.
16. Y.Y. Lin, Y. Peng, J.W. Di, *Sens. Actuat. B: Chem.*, 220 (2015) 1086.
17. H. Wang, Y.H. Zhang, H.M. Ma, X. Ren, Y.G. Wang, Y. Zhang, Q. Wei, *Biosens. Bioelectron.*, 86 (2016) 907.
18. N.J. Ronkainen, H.B. Halsall, W.R. Heineman, C*hem. Soc. Rev.*, 39 (2010) 1747.
19. L.L. Wang, T.M. Yao, S. Shi, Y.L. Cao, W. L. Sun, *Sci. Rep.*, 4 (2014) 5320.
20. Y.F. Pang, Z. Rong, R. Xiao, S.Q. Wang, *Sci. Rep.*, 5 (2015) 9451.
21. Z.D. Wang, J.H. Lee, Y. Lu, *Chem. Commun.*, 45 (2008) 6005.
22. D. Li, A. Wieckowska, I. Willner, *Angew. Chem.*, 5 (2008) 3991.
23. T.P. Qing, X.X. He, D.G. He, K.M. Wang, Y.L. Lei, T. Liu, P. Tang, Y. Li, *Talanta.*, 161 (2016) 170.
24. X. Zhao, J.S. Gao, X. He, L.C. Cong, H.M. Zhao, X.Y. Li, F. Tan, *RSC. Adv.*, 5 (2015) 39587.
25. R. Freeman, T. L. Finder, I. Willner, *Angew. Chem.*, 48 (2009) 7818.

26. K.T. Yong, I. Roy, H. Ding, E.J. Bergey, P.N. Prasad, *Small.*, 5 (2009) 1997.
27. G.F. Jie, Z.K. Lu, Y. Zhao, X.C. Wang, *Sens. Actuat. B. Chem.*, 240 (2017) 857.
28. F. Lu, S.H. Liu, L.P. Jiang, J.J. Zhu, *J. Nanopart. Res.*, 15 (2013) 1401.
29. E.K. Cho, A. Brown, T.F. Kuech, *Langmuir.*, 28 (2012) 11890.
30. Y. Wang, X. Bai, T.Y. Wang, L. Yan, T.Q. Zhang, Y. Zhang, W.W. Yu, *Nanotechnology.*, 28 (2017) 215703.
31. Z.Q. Li, C.J. Mo, Y. Guo, N.N. Xu, Q.Y. Zhu, D. Jie, *J. Mater. Chem. A.*, 5 (2017) 8519.
32. R.E. Bailey, S.M. Nie, *J. Am. Chem. Soc.*, 125 (2003) 7100.
33. W. Jiang, A. Singhal, J.N. Zheng, C. Wang, W.C.W. Chan, *Chem. Mater.*, 18 (2006) 4845.
34. P. Thomas, L. Nicolas, M. Benoit, S. Siarhei, F. Alexandra, D. Benoit, *Chem. Mater.*, 21 (2009) 1418.
35. B. Xing, W.W. Li, X.B. Wang, H.J. Dou, L. Wang, K. Sun, X.T. He, J.S. Han, H.S. Xiao, J.M. Miao, Y. Li, *J. Mater. Chem.*, 20 (2010) 5664.
36. R.B. Wang, O. Calvignanello, C.I. Ratcliffe, X.H. Wu, D.M. Leek, M.B. Zaman, D. Kingston, J.A. Ripmeester, K. Yu, *J. Phys. Chem. C.*, 113 (2009) 3402.
37. G.X. Liang, H.Y. Liu, J.R. Zhang, J.J. Zhu, *Talanta*, 80 (2010) 2172.
38. T. Pons, N. Lequeux, B. Mahler, S. Sasnouski, A. Fragola, B. Dubertret, *Chem. Mater.,* 21 (2009) 1418.
39. H. Peng, L.J. Zhang, C. Soeller, J. Travas-Sejdic, *J. Lumin.,* 127 (2007) 721.
40. J.K. Wu, Y.L. Yu, S.H. Wei, B. Xue, J.L. Zhang, *Int. J. Electrochem. Sci.,* 12 (2017) 11666.
41. M. Zhao, G.C. Fan, J.J. Chen, J.J. Shi, J.J. Zhu, *Anal. Chem.,* 87 (2015) 12340.
42. H.P. Huang, G.F. Jie, R.J. Cui, J.J. Zhu, *Electrochem. Commun.*, 11 (2009) 816.
43. H.M. Ma, Y.H. Zhao, Y.Y. Liu, Y. Zhang, D. Wu, H. Li, Q. Wei, *Anal. Chem.,* 89 (2017) 13049.
44. S.L.Tang, L.N. Wang, X.B. Feng, Z.H. Feng, R.Y. Li, H.P. Fan, K. Li, *Fuel*, 180 (2016) 194.
45. A. Cárdenas Valdivia, E. Vereda Alonso, M.M. López Guerrero, J. Gonzalez-Rodriguez, J.M. Cano Pavón, A. García de Torres, *Talanta,* 179 (2018) 1.
46. H. Bagheri, A. Gholami, *Talanta,* 55 (2001) 1141.